Research on Temperature Field Reconstruction Based on RBF Approximation with Polynomial Reproduction Considering the Refraction Effect of Sound Wave Paths

Qian Kong[1], Genshan Jiang[1, 2, *], Yuechao Liu[1]

[1] North China Electric Power University, Baoding, 071003, China

[2] State Key Laboratory of Acoustics, Institute of Acoustics, Chinese Academy of Sciences, Beijing, 100190, China

The temperature field distribution directly reflects the combustion condition in a furnace. In this paper, acoustic thermometry to reconstruct temperature distribution is investigated. A method based on radial basis function approximation with polynomial reproduction (RBF-PR) is proposed in order to improve the accuracy and stability of the method based on RBF approximation. In addition, the refraction effect of sound wave paths is considered in the process of reconstruction. The curved lines with refraction effect are numerically calculated by solving differential equations, which show that sonic waves curve towards the zones of higher temperature. The reconstructed performance is validated via numerical simulation using four temperature distribution models. Results and analysis show that the proposed method has much greater accuracy than the method based on RBF approximation, and when considering the effect of refraction, our method can reconstruct more excellent reconstruction performance than others, which do not take into account the refraction effect of sound wave paths.

Keywords: Acoustic thermometry; RBF, RBF with polynomial reproduction; refraction effect; sound wave paths.

1 Introduction

In the coal-fired boiler of large thermal power plant, the temperature distribution is one of the most important parameters of combustion process and equipment state.

The good combustion conditions can improve combustion efficiency, reduce coal consumption and emissions[1-3]. Therefore, the effective monitoring and controlling of the combustion temperature field in the furnace directly affect the safety and economy of the operation. However, the furnace provides a hostile and severely varying environment for combustion[4-6]. There is a lack of real-time, accurate and comprehensive methods to obtain temperature information for a long time. Therefore, it is very important and urgent to find an efficient method desired for measurement of the temperature fields in furnaces[7-9]. Acoustic method[10-13], as an advanced non-contact measurement, has advantages of real-time online monitoring and full-field measurement，and has good prospect of application in temperature field measurement of furnace.

Temperature distribution reconstruction using acoustic method is an inversion process, which depends greatly on reconstruction algorithm. Many algorithms have been proposed, such as the algorithm based on least square method (LSM)[14, 15], algorithm based on algebra reconstruction technique(ART)[16-18], and algorithm based on Radial Basis Function(RBF) approximation[19-21]. M. J. Wang et al.[14] applied the method based on LSM to reconstruct temperature distribution for circular area. S. P. Zhang et al.[17] used acoustic technology to monitor the temperature field of the cross-section in the boiler furnace, and the temperature profile was reconstructed through ART iteration. However, the algorithms based on LSM and ART are simple with quickness, but they have a limitation that the amount of divided blocks of measure area cannot exceed the number of effective wave paths, and the results they reconstructed lose much temperature information near the edge of measured area, while with low reconstruction accuracy. To make up for these defect, X. H. Shen et al.[19] presented the algorithm based on RBF approximation to reconstruct two-dimensional temperature field distribution, and validated the performance of temperature field reconstruction through four temperature distribution models. R. X. Jia et al.[20] used the method based on RBF approximation and gave the actual experiment. The results demonstrated that the method based on RBF approximation possessed a relatively better information reflection of temperature field distribution and higher reconstruction accuracy than common reconstruction algorithm, the least square method. However, the reconstruction algorithm based on RBF approximation has problems with stability and solvability. In addition, it requires a lot of training samples to calculate appropriate parameters of the neural network, while training samples are almost impossible to obtain in practice, even if obtained they are not accurate enough.

In addition, the temperature distribution in furnace is inhomogeneous, the temperature of the center is very high, while the temperature near the water wall tubes is very low, according to the acoustic principle, sound waves are no longer propagating in a straight line in the furnace[22-24]. When researchers commonly used acoustic thermometry to reconstruct the temperature field, the voice tracks often approximate straight lines. The errors because of refraction will influence the temperature field reconstruction. However seldom research has been done considering the refraction effect[25-27]. To ensure that measurements are accurate, it is necessary to take into account the effect of refraction of the sound wave.

In this paper, in order to overcome the shortcomings of above algorithms like low accuracy, or poor applicability, an improved reconstruction algorithm based on RBF approximation with polynomial reproduction (RBF-PR) is presented in this paper. In addition, we also consider the refraction effect of the sound wave paths in the process of temperature field reconstruction in Section 3. Section 4 utilizes four models with different complexity, including the one-peak symmetrical model, one-peak asymmetrical model, two-peak asymmetrical model and three-peak asymmetrical model, to validate the reconstruction performance of our proposed algorithm and gives experiment results and analysis. Conclusion is presented in Section 5.

2 The Theory of Acoustic Thermometry

The theory of acoustic thermometry is based on the relation between the velocity of sound and the temperature of fuel gas. The temperature can be obtained using the following relation:

$$u = \sqrt{\frac{\gamma R}{M}T} = Z\sqrt{T} \qquad (1)$$

Where u is the acoustic velocity in the medium, γ is the isentropic exponent of gas, R is the specific gas constant of an ideal gas, M is the molar mass and T is the absolute temperature. For a given gas mixture, γ, R, M are fixed constants and they can be replaced by Z. For example, in the air, Z is 20.03, and in the flue gas, Z is 19.98.

In the process of acoustic thermometry, when the distance d between the sound receiver and sound transmitter is known, and the time of flying (TOF) is measured, the velocity of sound can be calculated as

$$u = \frac{d}{\text{TOF}} \qquad (2)$$

Combine Equation (1), the temperature can be expressed by the following equation,

$$T = \left(\frac{d}{Z \cdot \text{TOF}}\right)^2 \qquad (3)$$

3 Reconstruction Method

3.1 Arrangement of Sound Transceivers and Division of the Measure area

A two-dimensional furnace system of $4m \times 4m$ being studied is shown in Figure 1. The space in the system is divided into 8×8 blocks by the dashed lines. The sound transceivers, A, B, C, D, E, F, P, Q, are installed around the perimeter of the measurement area to form a number of effective flying paths, which are represented by the solid lines. When transceiver A acts transmitters and radiates out sound signal, the other transceivers C, D, E, F, P, Q play the roles of receivers and detect the signal. When transceiver B radiates out the signal, the other transceivers C, D, E, F, P, Q act receivers. The cycle repeats and ends when Q emits the sound signal. Hence there will be 24 effective flying paths. The time of flying (TOF) of the paths is the same for the same path in the opposite direction, so each path is numbered only once. But in a practical experiment, the average TOF in opposite directions along the same path is often employed. When all TOF of the flying paths are obtained, the two-dimensional temperature distribution will be reconstructed by using suitable method.
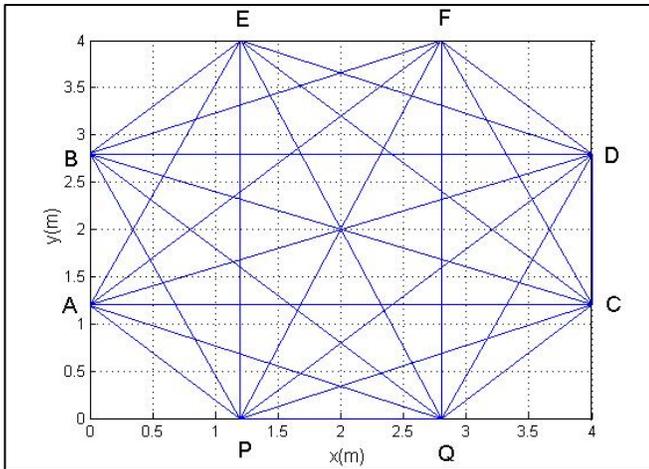
Figure 1. Arrangement of transceivers and division of the measure area.

3.2 The Method Based on RBF Approximation

If the measured area is divided into M blocks, (x_m, y_m) is the geometric center coordinate of the mth blocks, then the radial basis function whose center is located in (x_m, y_m) is expressed as:

$$\phi_m(x, y) = \frac{1}{\sqrt{(x - x_m)^2 + (y - y_m)^2 + C}} \qquad (4)$$

Where C is the shape parameter of RBF, which is related to the measured area and the arrangement of transceivers. It can be predetermined via numerical method, and in our model, RBF gives

the best result for shape parameter C=60.

The reciprocal of ultrasonic speed can be determined similarly as

$$f(x, y) = \sum_{m=1}^{M} \varepsilon_m \phi_m(x, y) \qquad (5)$$

Where the approximating function $f(x, y)$ is represented as a sum of M RBFs, each associated with a different reference point (x_m, y_m), and weighed by an appropriate coefficient ε_m.

The TOF, t_k in the kth effective acoustic flying path is described as

$$
\begin{aligned}
t_k &= \int_{l_k} f(x, y) dl_k = \int_{l_k} \sum_{m=1}^{M} \varepsilon_m \phi_m(x, y) dl_k \\
&= \sum_{m=1}^{M} \varepsilon_m \int_{l_k} \phi_m(x, y) dl_k = \sum_{m=1}^{M} \varepsilon_m a_{km}
\end{aligned}
\qquad (6)
$$

The linear system of Equation (6) can be represented as the matrix equation:

$$\mathbf{A\varepsilon} = \mathbf{t} \qquad (7)$$

And it can be also expressed in the form:

$$
\begin{pmatrix}
a_{11} & \cdots & a_{1M} \\
\vdots & \ddots & \vdots \\
a_{i1} & \cdots & a_{iM} \\
\vdots & \ddots & \vdots \\
a_{K1} & \cdots & a_{KM}
\end{pmatrix}
\begin{pmatrix}
\varepsilon_1 \\
\vdots \\
\varepsilon_M
\end{pmatrix}
=
\begin{pmatrix}
t_1 \\
\vdots \\
t_i \\
\vdots \\
t_K
\end{pmatrix}
\qquad (8)
$$

Where $a_{km} = \int_{l_k} \phi_m(x, y) \, dl_k$, K denotes the sum of effective paths, M is the number of blocks in measured area.

Thus matrix A is an ill condition one, i.e. the number of variables M is higher than the number of equations K. The linear system of equations(LSE) can be solved by the least squares method as

$$\mathbf{A^T A \varepsilon} = \mathbf{A^T t} \quad \text{or singular value decomposition, etc.}$$

3.3 Proposed Method Based on RBF-PR

The method which was introduced in Section 3.2 theoretically has problems with stability and solvability. Therefore the RBF approximant is usually extended by polynomial function

$$f(x, y) = \sum_{m=1}^{M} \varepsilon_m \phi_m(x, y) + P_k(x, y) \qquad (9)$$

In practice, a linear polynomial is used as

$$P_1(x, y) = a_x x + a_y y + a_0 \qquad (10)$$

Then TOF of the kth effective acoustic flying path

$$
\begin{aligned}
t_k &= \int_{l_k} f(x, y) dl_k = \int_{l_k} \sum_{m=1}^{M} \varepsilon_m \phi_m(x, y) + (a_x x + a_y y + a_0) dl_k \\
&= \sum_{m=1}^{M} \varepsilon_m \int_{l_k} \phi_m(x, y) dl_k + a_x \int_{l_k} x dl_k + a_y \int_{l_k} y dl_k + a_0 \int_{l_k} dl_k
\end{aligned}
\qquad (11)
$$

Using the matrix notation, we can write

$$
\begin{pmatrix}
a_{11} & \cdots & a_{1M} & b_{11} & b_{12} & c_1 \\
\vdots & \ddots & \vdots & \vdots & \vdots & \vdots \\
a_{i1} & \cdots & a_{iM} & b_{i1} & b_{i2} & c_i \\
\vdots & \ddots & \vdots & \vdots & \vdots & \vdots \\
a_{K1} & \cdots & a_{KM} & b_{K1} & b_{K2} & c_K
\end{pmatrix}
\begin{pmatrix}
\varepsilon_1 \\
\vdots \\
\varepsilon_M \\
a_x \\
a_y \\
a_0
\end{pmatrix}
=
\begin{pmatrix}
t_1 \\
\vdots \\
t_i \\
\vdots \\
t_K
\end{pmatrix}
\qquad (12)
$$

Where

$$a_{km} = \int_{l_k} \phi_m dl_k, \quad b_{k1} = \int_{l_k} x dl_k, \quad b_{k2} = \int_{l_k} y dl_k, \quad c_k = \int_{l_k} dl_k$$

The equation also can be expressed in the form:

$$(\mathbf{A} \quad \mathbf{B} \quad \mathbf{C}) \begin{pmatrix} \boldsymbol{\varepsilon} \\ \mathbf{a} \\ a_0 \end{pmatrix} = \mathbf{t} \tag{13}$$

It can be seen that now we have a linear system of equations in (M+3) variables compared with Equation (6). Thus the presented system has also ill-posed problem. And this LSE can be solved by the least squares method or singular value decomposition.

3.4 The Solution of Refraction of Sound Wave

According to the acoustic principle, when sound waves pass through non-uniform temperature field, they will bend because of refraction, and the greater the temperature gradient becomes, the more obviously sound waves curve. The temperature distribution in a furnace is inhomogeneous, so the temperature field should be reconstructed considering the effect of refraction of sound wave paths.

If the temperature distribution in the furnace is given in a furnace, the kth effective flying path of sound wave can be expressed as follows:

$$y_k = y_k(x) \tag{14}$$

The differential of the length s along this path is written as

$$ds = \left(1 + \left(\frac{dy}{dx}\right)^2\right)^{1/2} dx \tag{15}$$

So the TOF in the k-th flying path travelling from a transmitter $A(x_i, y_i)$ to a receiver $B(x_j, y_j)$ is described as

$$t_k = \int_A^B \frac{ds}{du} = \int_A^B \left(\frac{1}{(rR)^{1/2}} \frac{1 + y'^2}{T(x,y)}\right)^{1/2} dx \tag{16}$$

According to Fermat's theory, sound waves travel along the shortest path of the propagation time, so

$$t[y_k(x)] = \int_A^B F(x, y, y') = \int_A^B \frac{1}{(rR)^{1/2}} \left(\frac{1 + y'^2}{T(x,y)}\right)^{1/2} dx \tag{17}$$

Then the calculus of variations of Equation (17) should be zero

$$\delta(t[y_k(x)]) = \delta(\int_A^B F(x, y, y')) = 0 \tag{18}$$

Thus the Euler formula is obtained as

$$\frac{\partial F}{\partial y} - \frac{d}{dx}\left(\frac{\partial F}{\partial y'}\right) = 0 \tag{19}$$

Taking the function of $F(x, y, y')$ into Equation (19), the mathematical model of sound wave path in temperature field is established as

$$y'' = \frac{1}{2} \frac{1 + y'^2}{T(x,y)} \left(y' \frac{\partial T(x,y)}{\partial x} - \frac{\partial T(x,y)}{\partial y}\right) \tag{20}$$

and the boundary conditions can be expressed as follows,

$$\begin{cases} y_A = y(x)\big|_{x=x_A} \\ y_B = y(x)\big|_{x=x_B} \end{cases} \tag{21}$$

This is a two point boundary value problem of differential equation, it can be solved by shooting method or finite difference method.

3.5 The Process of Temperature Distribution Reconstruction

The procedure of proposed reconstruction method based on RBF-PR can be described in Figure 2.
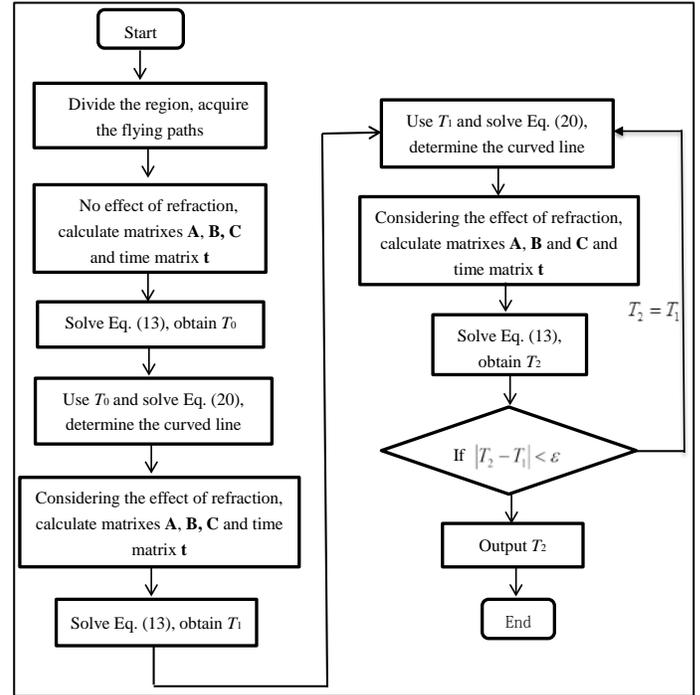
Figure 2. Flow chart of the proposed reconstruction method.

For practical experience, we can obtain matrix **t** via actual measurement. Then, the estimated matrix **t** can be applied into reconstruction method and the temperature field distribution would be reconstructed. But for simulation experiment in this paper, the model of temperature field distribution, which is artificially designed simulation environment could be expressed as a function. Then, matrix **t** in Equations (7) and (13) could be estimated. Finally, the reconstruction method based on RBF approximation and the proposed method based on RBF-PR can be applied to reconstruct the designed temperature field distribution.

4 Numerical Simulation and Results Analysis

In order to validate the performance of our proposed method, along all paths taking into account the refraction effect of sound wave in furnace, simulation experiments are carried out, and the results analysis is given. The TOF is assumed to be entirely accurate data which is obtained from theoretical calculation. In addition, the curved lines because of refraction effect can be obtained by solving the Equation (20), where T(x, y) is the value of temperature distribution models. The temperature field is then reconstructed using the TOF data with and without considering the refraction effect.

4.1 Design of Simulation and Definitions of Evaluation

As an improved method on the basis of RBF method, reconstruction results of the presented method based on RBF-PR are compared with that of method based on RBF. For convenience, the two methods are called RBF method and RBF-PR method in the subsequent sections, respectively.

In order to validate the capability of our proposed method and evaluate the reconstruction results, four kinds of two-dimensional temperature distribution models with different complexity levels are created. Then the TOF used in reconstruction is gained from these models via numerical computation, and we can make these models as standard of comparisons when temperature field is reconstructed. The expressions of these two-dimensional temperature distribution models created are shown as follows.

One-peak symmetrical temperature distribution:

$$T(x,y) = \frac{2000}{0.05((2.5x-5)^2 + (2.5y-5)^2) + 1} \tag{22}$$

One-peak asymmetrical temperature distribution:

$$T(x,y) = \frac{2000}{0.05((2.5x-7)^2 + (2.5y-7)^2) + 1} \tag{23}$$

Two-peak asymmetrical temperature distribution:

$$T(x,y) = 30 \times (\cos(2\pi(0.3x)^{1.1})\text{-}2) \times (\cos(2\pi(0.4y)^{1.1})\text{-}8) + 1800; \tag{24}$$

Three-peak asymmetrical temperature distribution:

$$\begin{aligned}T(x,y) = 800 + 1000\exp&\left[-20\left(\frac{x}{4}-\frac{1}{5}\right)^2 - 20\left(\frac{3y}{11}-\frac{5}{7}\right)^2\right]\\ + 1000\exp&\left[-20\left(\frac{x}{4}-\frac{4}{5}\right)^2 - 20\left(\frac{3y}{11}-\frac{4}{7}\right)^2\right]\\ + 1000\exp&\left[-20\left(\frac{x}{4}-\frac{2}{5}\right)^2 - 15\left(\frac{3y}{11}-\frac{1}{3}\right)^2\right]\end{aligned} \tag{25}$$

For the sake of comprehensive evaluation, not only qualitative analysis but also quantitative analysis is provided. The former is given as figures of isothermal contour displays, their corresponding absolute errors and the refracted sound waves. The latter include TOF of effective paths with and without considering refraction effect, and temperature error analysis, which is given by calculating the maximum error E_{max}, mean relative error E_{mean} and root-mean-square percent error E_{rms},

$$E_{max} = \max|T(m) - T'(m)|$$

$$E_{mean} = \frac{\sum_{m=1}^{P}\left|\frac{T(m)-T'(m)}{T(m)}\times 100\%\right|}{P} \tag{26}$$

$$E_{rms} = \frac{\sqrt{\frac{1}{P}\sum_{m=1}^{P}(T(m)-T'(m))^2}}{T_{mean}}\times 100\%$$

Where P is the number of calculated points, $T(m), T'(m)$ is temperatures of point (x_m, y_m) respectively of model one and reconstructed one. T_{mean} is the mean temperature of model.

4.2 Simulation Results and Analysis

Figures 3-6 show the reconstructed results for one-peak symmetrical temperature distribution, one-peak asymmetrical one, two-peak asymmetrical one, and three-peak asymmetrical one. (a), (c1), (d1) in Figures 3-6 show the isothermal contour displays of temperature distribution models, the corresponding reconstructed ones respectively, gained using RBF method and our proposed RBF-PR method without considering the effect of refraction. (e1) in Figures 3-6 show the isothermal contour displays of reconstructed temperature distribution with considering the refraction effect. (c2), (d2), (e2) in Figures 3-6 show the absolute errors of the temperature distributions reconstructed using RBF, RBF-PR method without taking into account the effect of refraction, and RBF-PR method with considering the effect. Moreover, paths with refraction are shown in Figure (b).

For simple one-peak symmetrical and one-peak asymmetrical temperature distribution, without considering the refraction effect, the reconstruction based on our proposed RBF-PR method conforms better to their models, comparing with one based on RBF method. And with considering the refraction effect, we can gain the best result based on RBF-PR method. In addition, for one-peak symmetrical

temperature distribution, the absolute errors of RBF-PR method are small, almost all of which are below 10 K. While the errors of RBF are obvious larger, especially near the four corners where error is nearly 150 K. For one-peak asymmetrical temperature distribution, reconstruction of that is more difficult than reconstruction of a symmetrical one. The absolute errors show that the accuracy of the results based on RBF-PR method is improved remarkably compared with RBF method. The error of RBF method is around 100 K in most area, while it will dramatically increase to about 300 K near the corner at point (4, 4). However, in the proposed method, the most area's error and the maximum error are reduced to about 10 K and 50 K, respectively.

For two-peak asymmetrical model and three-peak asymmetrical model, the temperature distributions gradually get much more complex, so the spatial resolution is apt to deteriorate. Therefore, it is important to demonstrate the possibility of reconstructing these temperature fields. From the isothermal contour displays of reconstructed temperature distribution and absolute errors, the simulation results indicate that all of these reconstruction algorithms can solve the complex models. For two-peak asymmetrical model, the results of RBF-PR method have more excellent reconstruction performance than ones of RBF method, but for three-peak asymmetrical model, absolute errors of RBF-PR method are a little larger than that of RBF method. In general, the method based on RBF-PR with considering the effect of refraction is the best reconstruction algorithm for these two complex models.

Figures 3(b), 4(b), 5(b) and 6(b) show the sound wave paths because of refraction effect for one-peak symmetrical model, one-peak asymmetrical model, two-peak asymmetrical model and three-peak asymmetrical model. The simulation results show that sound waves do not propagate in along straight lines in fields of non-uniform temperature. For one-peak symmetrical model and one-peak asymmetrical one, the temperature gradient changes large, so the sound waves curve towards the peak and refraction becomes strong near the peak. For two-peak asymmetrical model, because the temperature gradient changes little, the curved lines look like the straight lines. But in the case of three-peak asymmetrical temperature distributions, the refraction becomes more complex, as shown in Figure 6(b). In conclusion, the sound waves curve towards the zones of higher temperature in these four models, and when the temperature gradient varies greatly, the sound waves curve obviously.

Table 1. TOF of 6 paths for one-peak symmetrical temperature distribution.

Paths	TOF/s	TOF/s
	No considering curved line	Considering curved line
P-A	0.00301592	0.00298941
P-B	0.00499927	0.00486113
P-C	0.00499927	0.00489076
P-D	0.00589534	0.00581012
P-E	0.00592251	0.00584115
P-F	0.00608685	0.00608692

(a)

(b)

(c1)
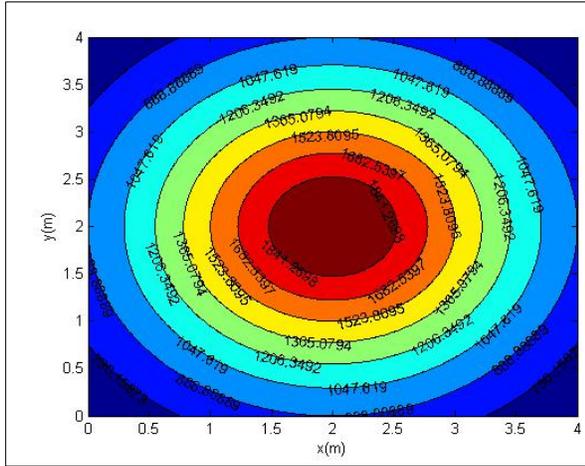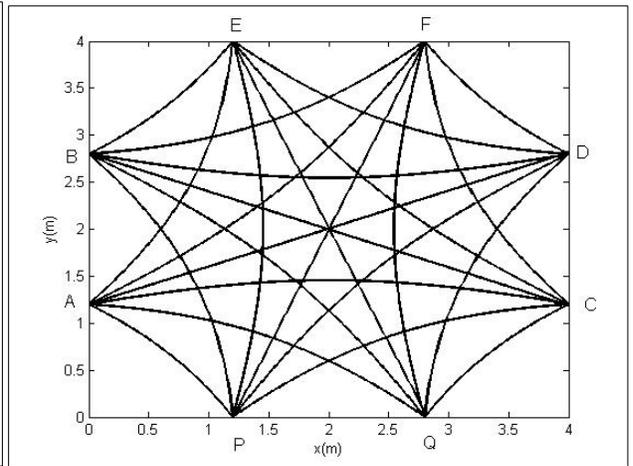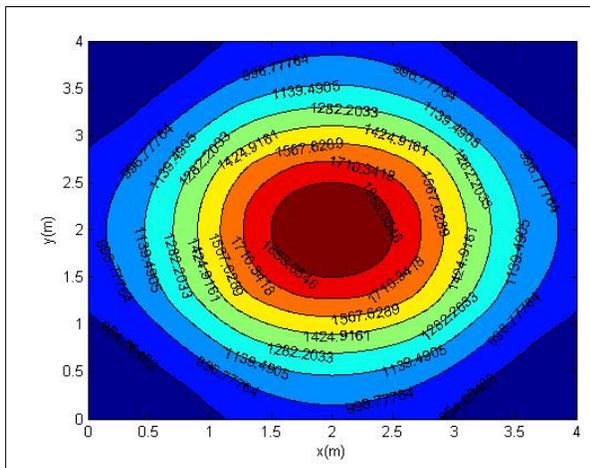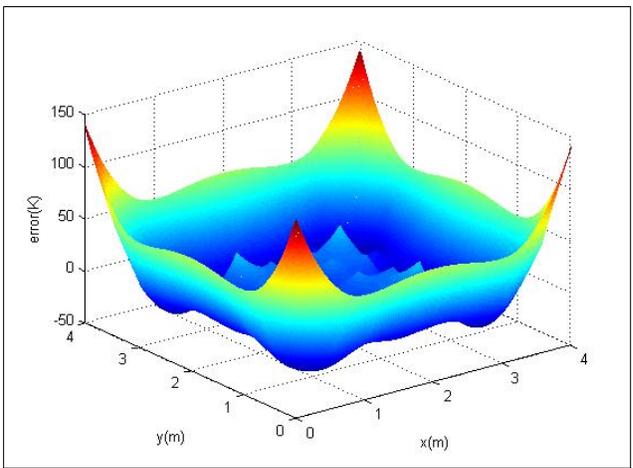
(c2)
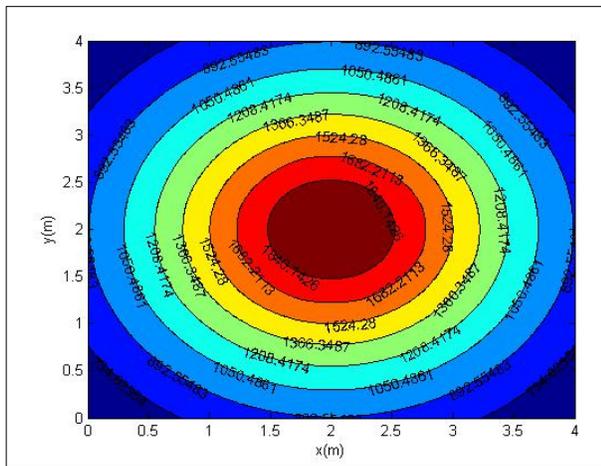
(d1)
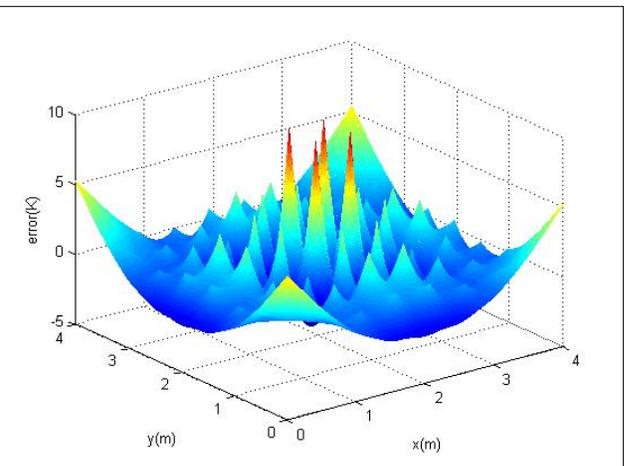
(d2)
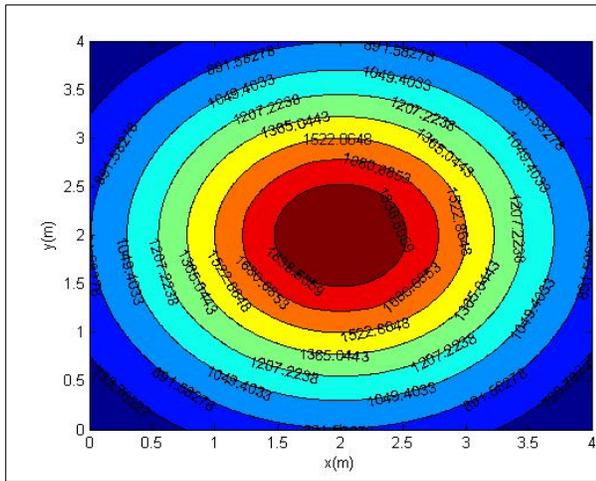
(e1)
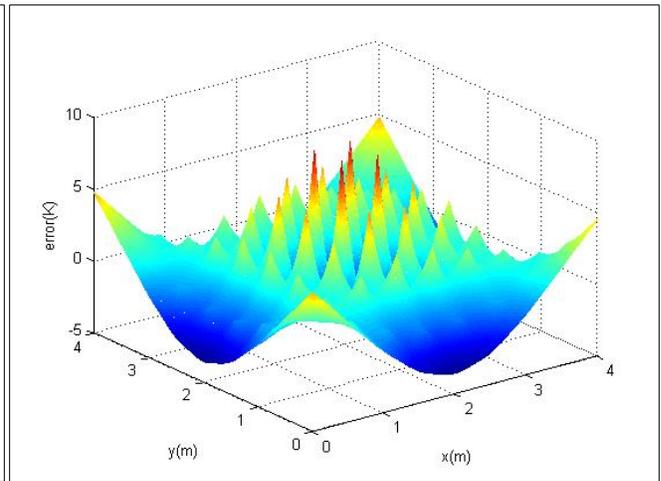
(e2)

Figure 3. The reconstruction results for one-peak symmetrical temperature distribution.

(a)

(b)

(c1)
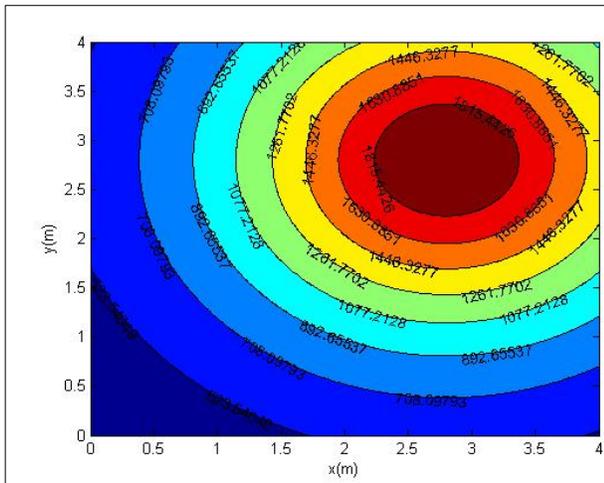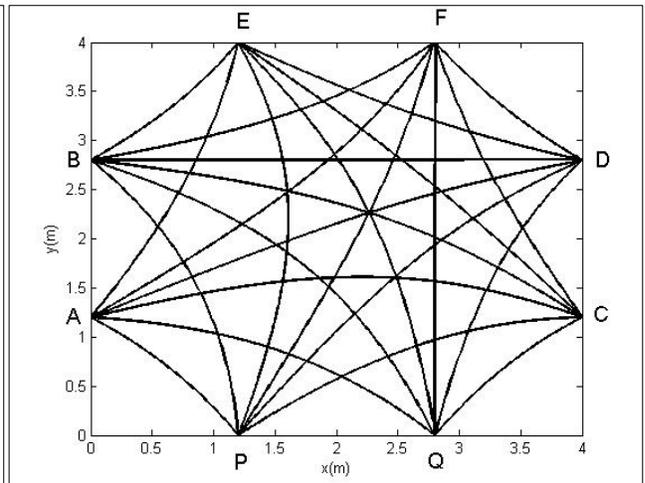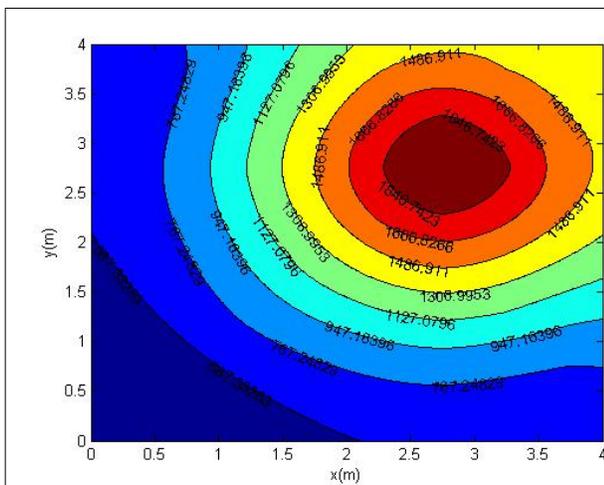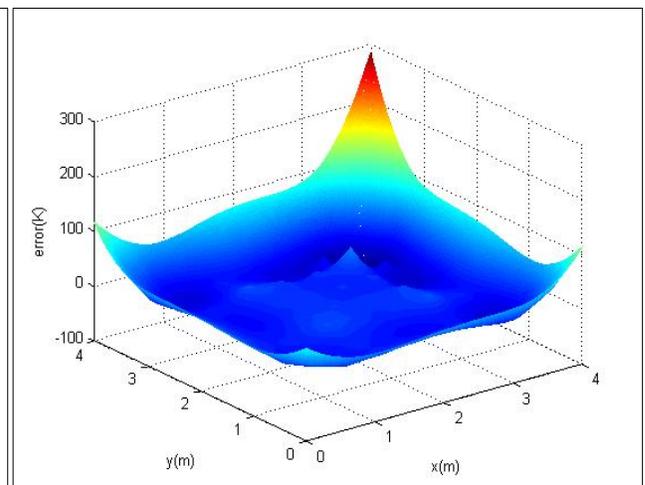
(c2)
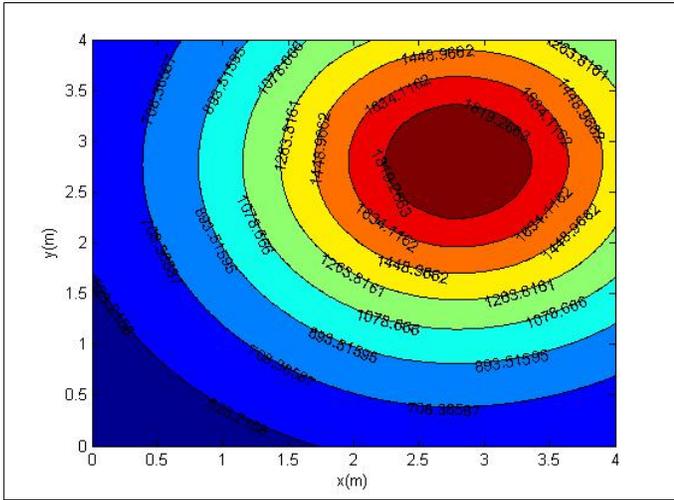
(d1)
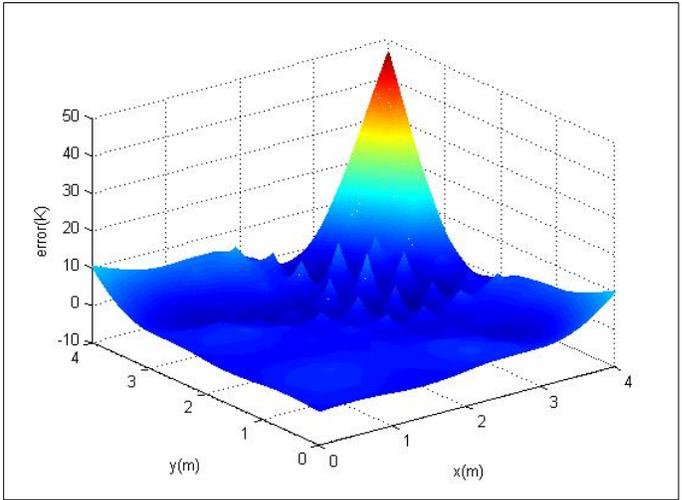
(d2)
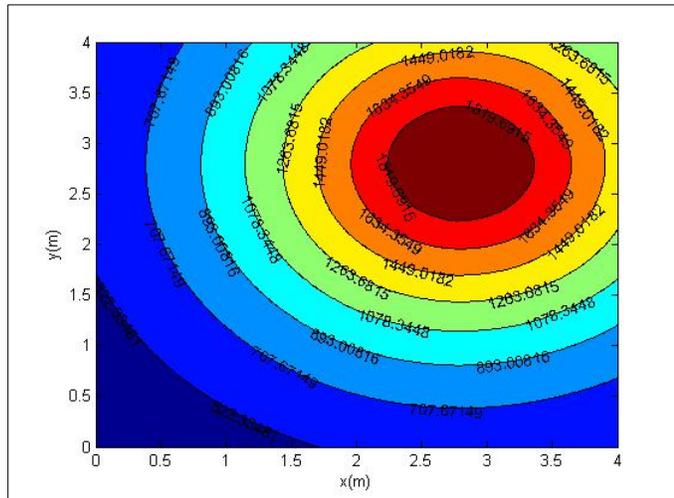
(e1)
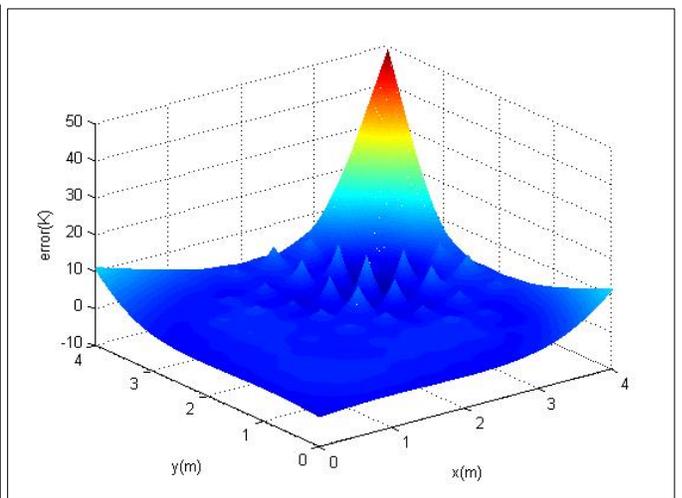
(e2)

Figure 4. The reconstruction results for one-peak asymmetrical temperature distribution.

(a)

(b)

(c1)
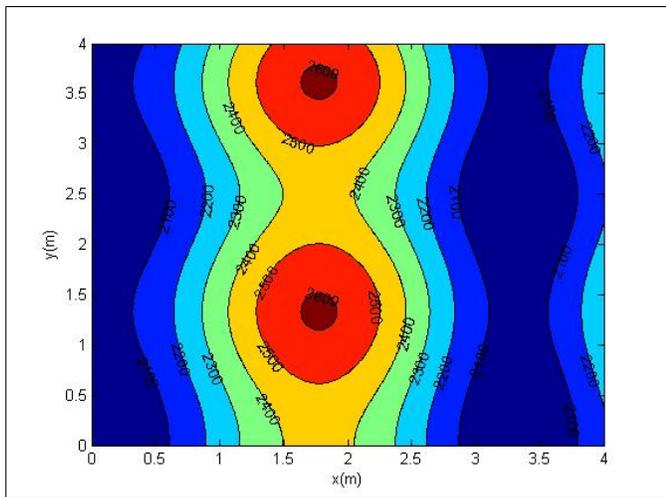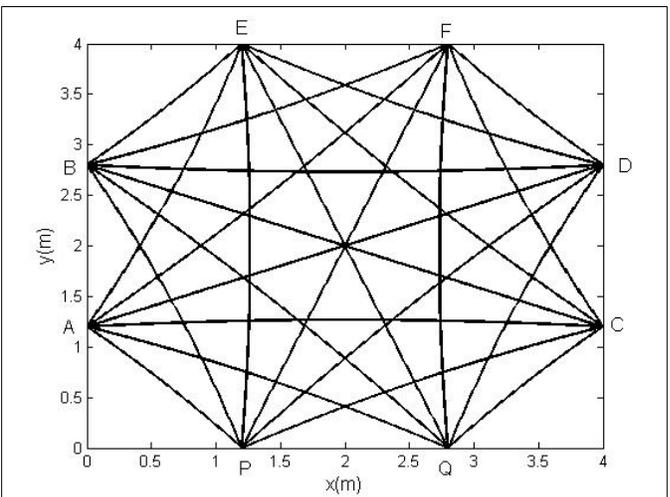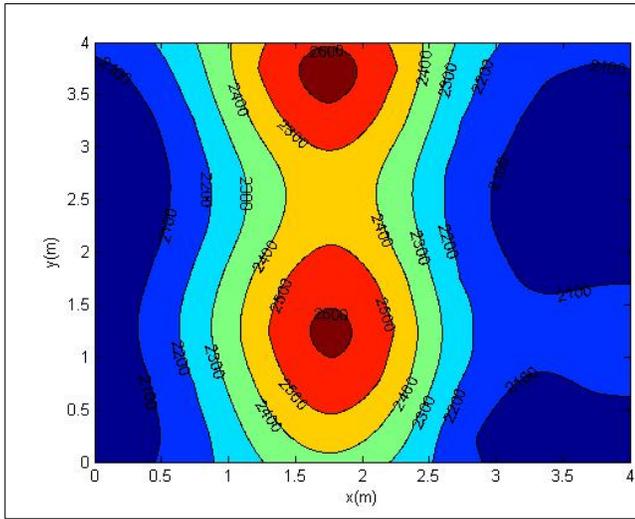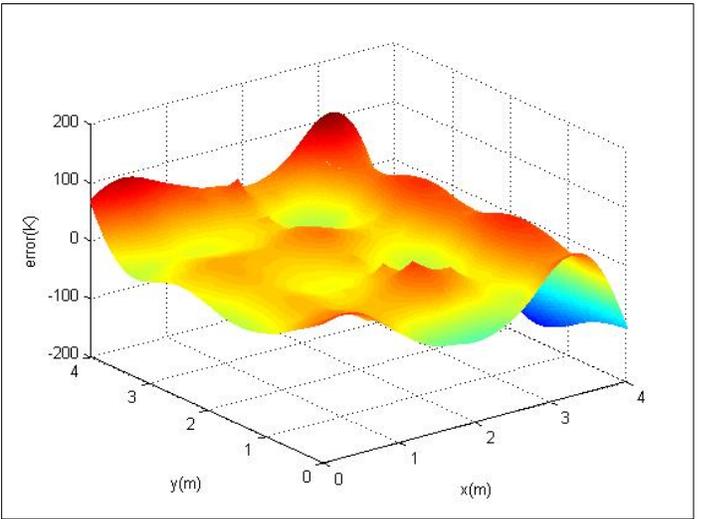
(c2)
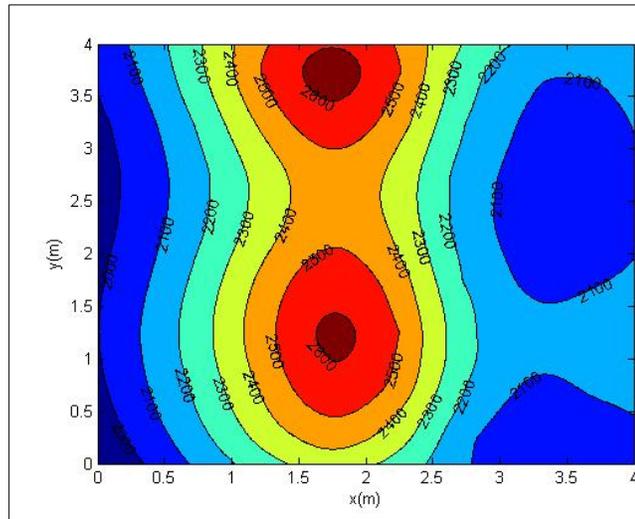
(d1)
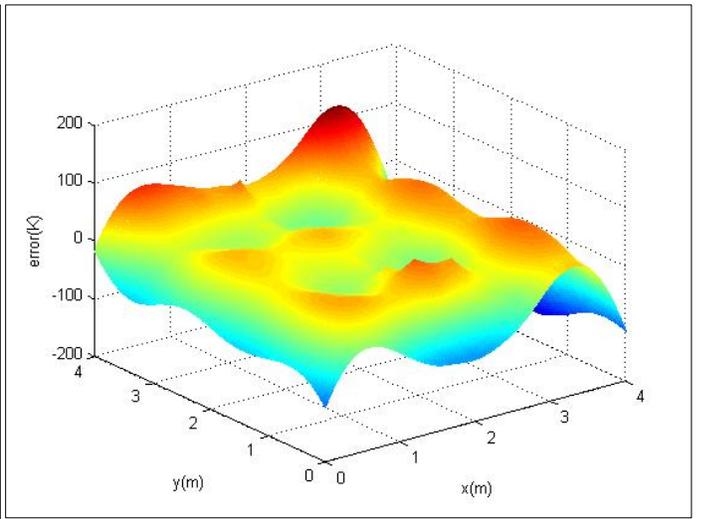
(d2)
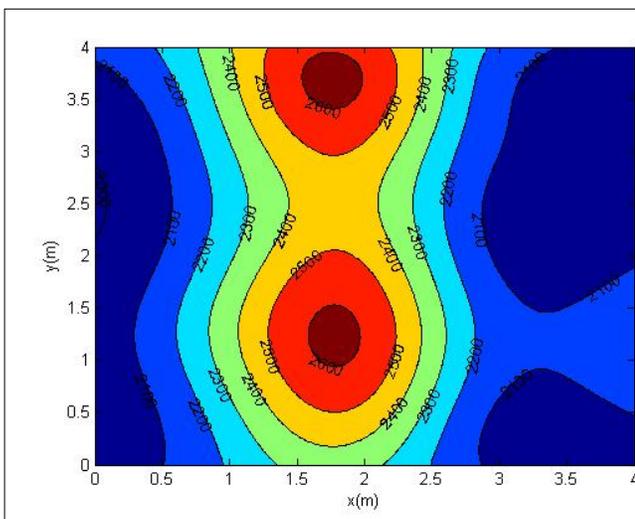
(e1)
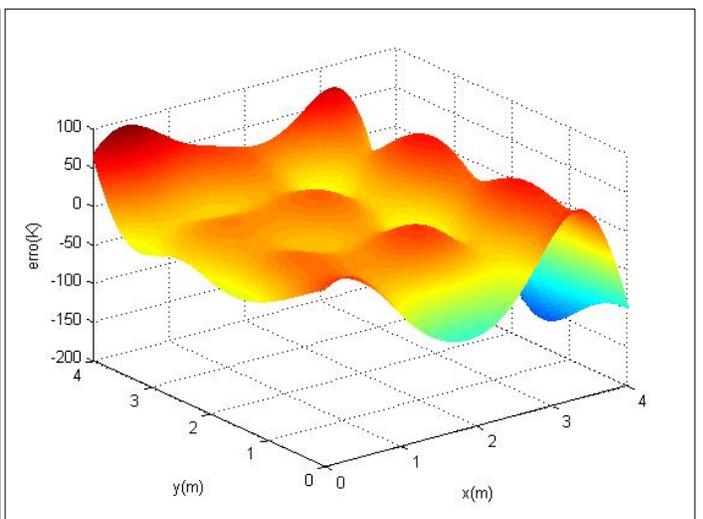
(e2)

Figure 5. The reconstruction results for two-peak asymmetrical temperature distribution.

(a)

(b)

(c1)
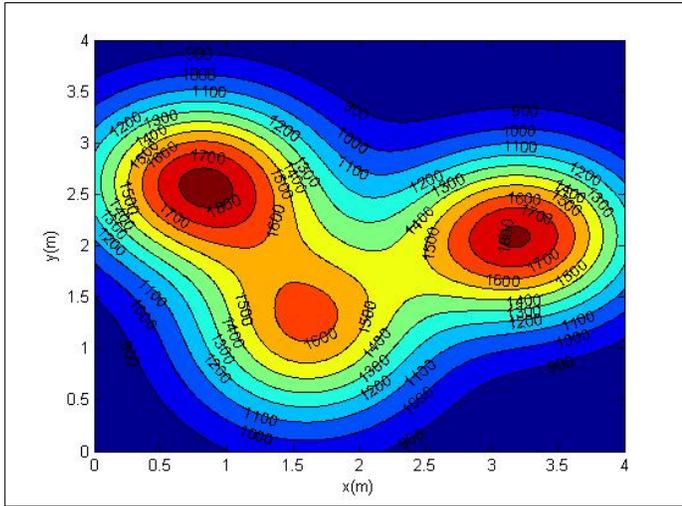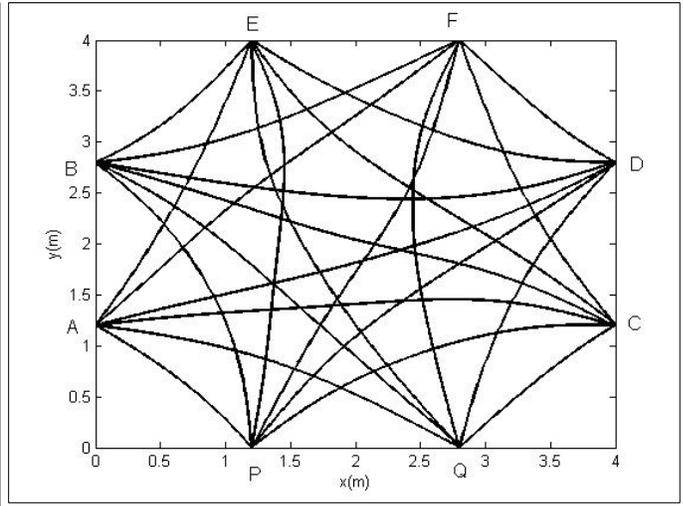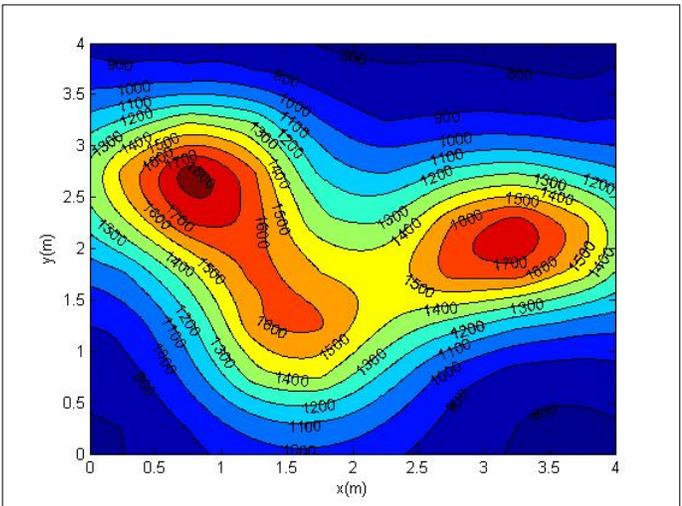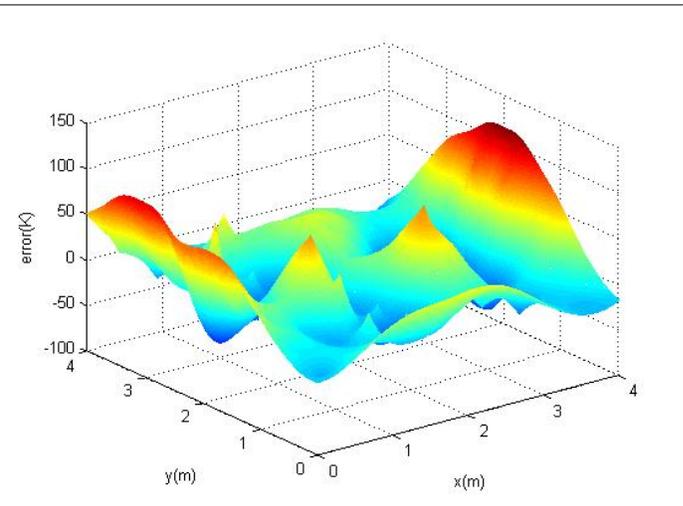
(c2)
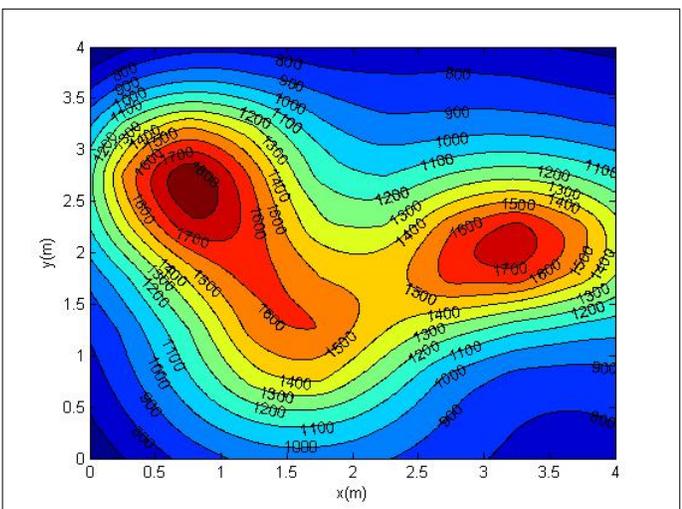
(d1)
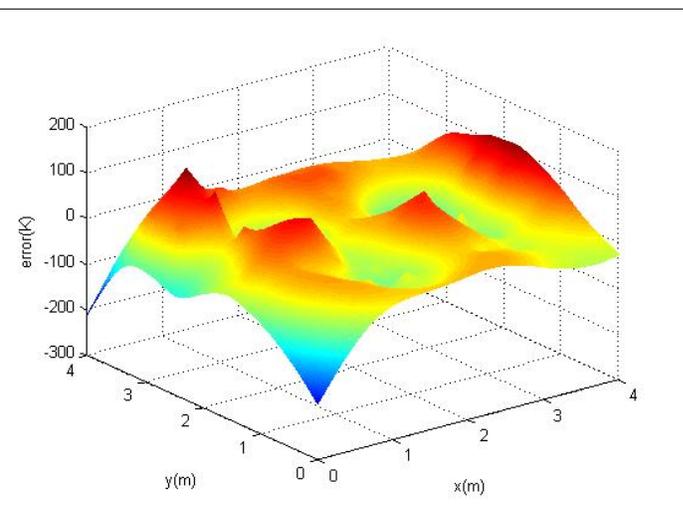
(d2)
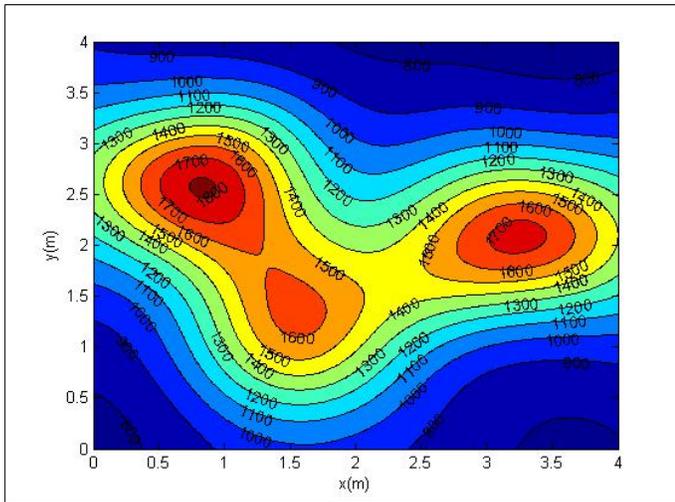
<div style="text-align:center">(e1)</div>
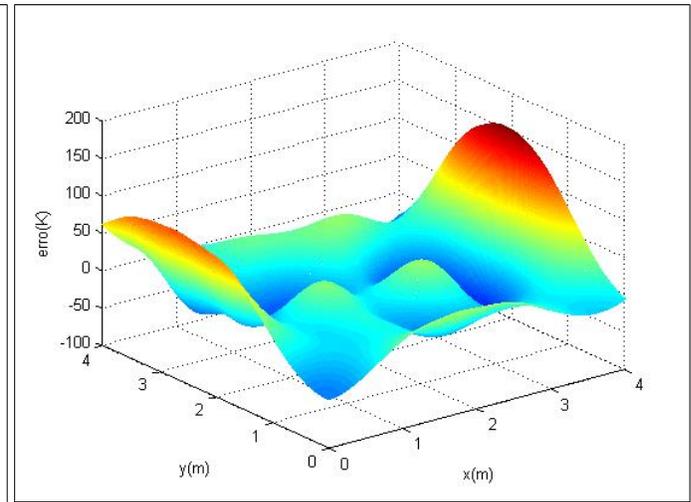
<div style="text-align:center">(e2)</div>

Figure 6. The reconstruction results for three-peak asymmetrical temperature distribution.

Table 2. TOF of 24 paths for one-peak asymmetrical temperature distribution.

Paths	TOF/s No considering curved line	TOF/s Considering curved line	Paths	TOF/s No considering curved line	TOF/s Considering curved line
P-A	0.00402698	0.00399934	A-C	0.00722476	0.00701705
P-B	0.0065449	0.00638527	A-D	0.00675334	0.00672526
P-C	0.00590707	0.00579383	A-E	0.00590707	0.0052281
P-D	0.00648111	0.00641189	A-F	0.00648111	0.00641372
P-E	0.00722473	0.00701705	B-C	0.00686347	0.0067218
P-F	0.00675334	0.00676683	B-D	0.00584672	0.00584675
Q-A	0.0065425	0.00639943	B-E	0.0032633	0.00324319
Q-B	0.00751311	0.00724488	B-F	0.00495368	0.00489276
Q-C	0.0032633	0.00324355	C-E	0.00551278	0.0054958
Q-D	0.00495368	0.00490481	C-F	0.00415002	0.00412357
Q-E	0.00686347	0.00658871	D-E	0.00414655	0.00413353
Q-F	0.00584668	0.00584675	D-F	0.00226689	0.0022573

Table 3. TOF of 24 paths for two-peak asymmetrical temperature distribution.

Paths	TOF/s No considering curved line	TOF/s Considering curved line	Paths	TOF/s No considering curved line	TOF/s Considering curved line
P-A	0.00191844	0.00191829	A-C	0.00438293	0.00438262
P-B	0.00343703	0.0034319	A-D	0.00477678	0.00477463
P-C	0.00336496	0.00336294	A-E	0.0034266	0.0034218
P-D	0.00436078	0.00435639	A-F	0.00432253	0.00431913
P-E	0.00428606	0.00438262	B-C	0.00478288	0.00477968
P-F	0.00459303	0.00458691	B-D	0.00446844	0.00446586
Q-A	0.00334103	0.00333915	B-E	0.00190204	0.00190173
Q-B	0.00432565	0.00432331	B-F	0.00330257	0.00330231
Q-C	0.00194421	0.00194417	C-E	0.00434463	0.00434235
Q-D	0.0034922	0.00349063	C-F	0.00347838	0.00347773
Q-E	0.00459115	0.00456272	D-E	0.00332701	0.00332624
Q-F	0.00449756	0.00446586	D-F	0.00193466	0.0019342

Table 4. TOF of 24 paths for three-peak asymmetrical temperature distribution.

Paths	TOF/s No considering curved line	TOF/s Considering curved line	Paths	TOF/s No considering curved line	TOF/s Considering curved line
P-A	0.00292151	0.00290392	A-C	0.00602931	0.00594776
P-B	0.00467187	0.00452164	A-D	0.00617421	0.00612072
P-C	0.00509203	0.00495465	A-E	0.00455882	0.00454114
P-D	0.00565507	0.00558556	A-F	0.00621782	0.00621132
P-E	0.00577080	0.00594776	B-C	0.00592607	0.00591028
P-F	0.00662893	0.00660903	B-D	0.00581635	0.00564619
Q-A	0.00493928	0.00486723	B-E	0.00266068	0.00263150
Q-B	0.00566595	0.00560000	B-F	0.00489075	0.00484266
Q-C	0.00303575	0.00303072	C-E	0.00608661	0.00603406
Q-D	0.00477010	0.00471250	C-F	0.00473308	0.00470725
Q-E	0.00669331	0.00656406	D-E	0.00528703	0.00520682
Q-F	0.00632777	0.00564619	D-F	0.00298363	0.00297730

Table 5. Errors of methods with and without refraction effect.

Model	Method		$E_{\max}$	E_{mean}	E_{rms}
			(K)	(%)	(%)
One-peak symmetrical model	Without refraction effect	RBF	139.9	2.09	2.21
		RBF-PR	5.3	0.11	0.13
	With refraction effect	RBF-PR	4.6	7.9e(-4)	0.1
One-peak asymmetrical model	Without refraction effect	RBF	283	1.92	2.66
		RBF-PR	46	0.21	0.40
	With refraction effect	RBF-PR	48	0.17	0.38
Two-peak asymmetrical model	Without refraction effect	RBF	204	1.63	2.02
		RBF-PR	170	1.08	1.47
	With refraction effect	RBF-PR	137	0.9	1.36
Three-peak asymmetrical model	Without refraction effect	RBF	113	1.80	2.34
		RBF-PR	216	2.73	3.38
	With refraction effect	RBF-PR	132	1.75	2.28

Tables 1-4 show the TOF of paths without and with considering the effect of refraction based on RBF-PR method, respectively. Due to the symmetry of one-peak symmetrical model, the TOF of 6 paths are given in Table 1, while TOF of 24 paths are listed for other models. The results shown in tables indicate that TOF of most of curved paths with refraction effect is shorter than that without refraction effect, although few curved paths cost a little longer time than line paths.

Table 5 shows the maximum error $E_{\max}$, mean relative error E_{mean} and root-mean-square percent error E_{rms} of reconstructions based on RBF method, and RBF-PR method with and without refraction effect for the four temperature distribution models, it can be seen that most errors of RBF method are larger than that of our proposed method RBF-PR. For one-peak symmetrical and asymmetrical temperature distribution, when considering the effect of refraction, the errors is a littler smaller than that without refraction effect. In addition, the mean relative error E_{mean} and root-mean-square percent error E_{rms} are below 0.1% for one-peak symmetrical model, and these errors are within 0.38% for one-peak asymmetrical model with the refraction effect. However, for the two-peak asymmetrical models, the errors decrease obviously under the same condition. For complex three-peak asymmetrical models, although the errors of our proposed RBF-PR method are larger than that of RBF without refraction effect, when considering the refraction effect, the errors decreases. In conclusion, the proposed RBF-PR method with refraction effect has relatively higher reconstruction accuracy than ones without refraction effect in these four temperature distribution models.

5 Conclusions

In this paper, an improved method based on RBF-PR is presented to reconstruct temperature distribution in a furnace, and in the process of temperature distribution reconstruction, the refraction effect of sound wave path is taken into account. The performance of proposed method is validated via numerical simulation using four temperature distribution models. On the basis of the experiment results, we can have the following conclusions,

(1) Without considering the effect of refraction, the presented method based on RBF-PR can improve the reconstruction performance compared with the method based on RBF approximation.

(2) Sound waves do not propagate along the straight lines in fields of non-uniform temperature, while they curve towards the zones of higher temperature, and the greater the temperature gradient becomes, the more obviously sound waves curve.

(3) In the four temperature distribution models with different complexity, the accuracy of reconstructed temperature fields, obtained by the RBF-PR method is all improved when taking the refraction effect of sound wave paths into account.

References
1. Xu, T. M., Zhao, Q. X., Hui, S. E., "Status and trend on boiler safety SCI-tech research in China," China Special Equipment Safety, Vol. 22, pp. 3-8, 2006.
2. Feron, P. H. M., "Exploring the potential for improvement of the energy performance of coal fired power plants with post-combustion capture of carbon dioxide," International Journal of Greenhouse Gas Control, Vol. 4, pp. 152-160, 2010.
3. Galletti, C., Parente, A., Tognotti, L., "Numerical and experimental investigation of a mild combustion burner," Combustion and Flame, Vol. 151, pp. 649-664, 2007.
4. Derichs, W., Menzel, F., Reinartz, K., "Acoustic pyrometry: A correlation between temperature distributions and the operating conditions in a brown coal fired boiler," 2nd International Conference on Combustion Technologies for A Clean Environment, Lissabon, 1993.
5. Shang, Q. Y., "Current status and development trend of pulverized coal industrial boilers in China," Coal Science and Technology, Vol. 44, 201-206, 2016.
6. Liu, F. Q., "The present situation and development trend of industrial boiler," Applied Energy Technology, Vol. 5, pp. 19-20, 2014.
7. Bramanti, M., Salerno, E. A., Tonazzini, A., Pasini, S., "An acoustic pyrometer system for tomographic thermal imaging in power plant boilers," IEEE Transactions on Instrumentation & Measurement, Vol. 45, 159-167, 1996.
8. Muzio, L., Eskinazi, D., Green S., "Acoustic pyrometry: New boiler diagnostic tool," Power Engineering, Vol. 93, pp. 49-52, 1989.
9. Hanson, T. A., Yilmaz, N., Drozda, P., "Acoustic pyrometry using an off-the-shelf range finding system," Journal Fire

Science, Vol. 26, pp. 287-308, 2008.

10. Gade, S., Hald, J., Ginn, K. B., "Wideband acoustical holography," Sound and Vibration, pp. 8-13, 2016.

11. Srinivasan, K., Sundararajan, T., Narayanan, S., Jothi, T. J. S., Sarma, C. S. L. V. R., "Acoustic pyrometry in flames", Measurement, Vol. 46, 315-323, 2013.

12. Barth, M., Raabe, A., "Acoustic tomographic imaging of temperature and flow fields in air," Measurement Science & Technology, Vol. 22, pp. 1-13, 2011.

13. Tian, F., Shao, F. Q., Wang, F. L., "Comprehensive survey of temperature field detection techniques used acoustic in Furnace," Instrument Technique and Sensor, Vol. 4, pp. 52-54, 2002.

14. Wang, M. J., Zhang, L. W., Cao, W., "Simulation study on two-dimensional temperature field of circular boundary by acoustic measurement," Science Technology and Engineering, Vol. 10, pp. 3848-3851, 2010.

15. Shen, G. Q., An, L. S., Jiang, G. S., Simulation of two-dimensional temperature field in furnace based on acoustic computer tomography, Proceeding of the CSEE, Vol. 27, pp. 11-14, 2007.

16. Tian, F., Shao, F., Wang, F., "Complex temperature field reconstruction algorithm based on combination of regularzation method and iterative technology," North-East Asia IT Symposium, pp. 1, 2002.

17. Zhang, S. P., Shen, G. Q., An, L. S., Niu, Y. G., "Online monitoring of the two-dimensional temperature field in a boiler furnace based on acoustic computed tomography," Applied Thermal Engineering, Vol. 75, pp. 956-966, 2015.

18. Xie, L. B., Liu, T., Zhang, Z. G., Shao, W., "The 2-D temperature reconstruction based on the algorithm of interpolation and iterative," Proceeding of the CSEE, Vol. 24, pp. 249-252, 2004.

19. Shen, X. H., Xiong, Q. Y., Shi, X, Wang, K., Liang, S. "Ultrasonic temperature distribution reconstruction for circular area based on Markov radial approximation and singular value decomposition," Ultrasonic, Vol. 62, pp. 174-185, 2015.

20. Tian, F., Liu, Z. S., Sun, X. P., Shao, F., "Temperature field reconstruction algorithm based on RBF neural network," Chinese Journal of Scientific Instrument, Vol. 27, pp. 1460-1464, 2006.

21. Jia, R. X, Xiong, Q. Y., Xu, G. Y., Wang, K., Liang, S., "A method for two-dimensional temperature field distribution reconstruction," Applied Thermal Engineering, Vol. 111, pp. 961-967, 2017.

22. Tarau, C., Otugen, M. V., "Propagation of acoustic waves through regions of non-uniform temperature," Aeroacoustics, Vol. 2, pp. 165-181, 2002.

23. Lekner, J., "Reflection and transmission of compressional waves by a stratification with discontinuities in density and sound speed," Acoustic Society of America, Vol. 88, pp. 2876-2879, 1990.

24. Tian, F., Zhao F. Q., Wang, F. L., Chen, S., "Simulation of complex temperature field reconstruction algorithm based on curved paths," Journal of System Simulation, Vol. 15, pp. 621-623, 2003.

25. Lu, J., Wakai, K., Takahashi, S., Shimizu, "Acoustic computer tomographic pyrometry for two-dimensional measurement of gases taking into account the effect of refraction of sound wave paths," Measurement Science and Technology, Vol. 11, pp. 692-697, 2000.

26. Jiang, G. S., An, L. S., Yang, K., "Numerical study on the propagation path of sound ray through the temperature gradient field," Proceeding of the CSEE, Vol. 24, pp. 210-214, 2004.

27. Yan, H., Wang, S. H., Liu, L. J., Zhou, Y. G., "A reconstruction algorithm of temperature field taking into account the bending of sound wave paths," Acta Acustica, Vol. 39, pp. 705-713, 2014.

The author can be reached at: gsjiang@ncepu.edu.cn.